CORA Cork Open Research Archive
Cartlann Taighde Oscailte Chorcaí

Title	Assessing the intrinsic radiation efficiency of tissue implanted UHF antennas
Authors	El-Saboni, Yomna;Zelenchuk, Dmitry E.;Conway, Gareth A.;Scanlon, William G.
Publication date	2019-08-19
Original Citation	El-Saboni, Y., Zelenchuk, D. E., Conway, G. A. and Scanlon, William G. (2019) 'Assessing the intrinsic radiation efficiency of tissue implanted UHF antennas', IEEE Transactions On Antennas and Propagation, 68(1), pp. 491-499. https://doi.org/10.1109/TAP.2019.2935113
Type of publication	Article (peer-reviewed)
Link to publisher's version	10.1109/TAP.2019.2935113
Rights	© 2019 IEEE. Personal use of this material is permitted. Permission from IEEE must be obtained for all other uses, in any current or future media, including reprinting/republishing this material for advertising or promotional purposes, creating new collective works, for resale or redistribution to servers or lists, or reuse of any copyrighted component of this work in other works.
Download date	2026-11-03 01:11:11
Item downloaded from	https://hdl.handle.net/10468/8284

UCC
University College Cork, Ireland
Coláiste na hOllscoile Corcaigh

Assessing the Intrinsic Radiation Efficiency of Tissue Implanted UHF Antennas

Yomna El-Saboni, *Student Member, IEEE*, Dmitry E Zelenchuk, *Senior Member, IEEE*, Gareth A. Conway, *Senior Member, IEEE* and William G. Scanlon, *Senior Member, IEEE*

***Abstract*—Dielectric loss occurring in tissues in close proximity to UHF implanted antennas is an important factor in the performance of medical implant communication systems. Common practice in numerical analysis and testing is to utilize radiation efficiency measures external to the tissue phantom employed. This approach means that radiation efficiency is also dependent on the phantom used and antenna positioning, making it difficult to understand antenna performance and minimize near-field tissue losses. Therefore, an alternative methodology for determining the intrinsic radiation performance of implanted antennas that focuses on assessing structural and near field tissue losses is presented. The new method is independent of the tissue phantom employed and can be used for quantitative comparison of designs across different studies. The intrinsic radiation efficiency of an implant antenna is determined by assessing the power flow within the tissue phantom at a distance of at least $\lambda_g/2$ from the radiating structure. Simulated results are presented for canonical antennas at 403 MHz and 2400 MHz in homogeneous muscle and fat phantoms. These illustrate the dominance of propagating path losses in high-water content tissues such as muscle, whereas near-field dielectric losses may be more important in low-water tissues such as fat due to the extended reactive near-field.**

***Index Terms*—Antenna efficiency; radiation efficiency; implantable antennas; reactive near-field; path loss; antenna characterization**

I. Introduction

INTEREST in the field of Wireless Implantable Medical Devices (WIMDs) is increasing due to the range of potential medical applications. Examples include minimally invasive sensing and monitoring of transplanted organs to improve both medical diagnosis and treatment and to simultaneously provide patients with a more independent lifestyle [1]–[4]. WIMD based solutions are also relevant to new forms of brain interfacing and neuro-stimulators including urinary bladder control, the early detection and interruption of seizures or when monitoring brain functionality in patients diagnosed with Alzheimer's disease or related illnesses. Similarly, WIMDs have a role to play in directly improving patient quality of life through smart prosthesis or artificial organs [5]–[7].

Irrespective of the application it is clear that wireless communication with implanted medical devices is advantageous as it reduces the risk of infection [8] and offers much more flexibility in terms of selection of the implant site [5], [9]. Early medical implants utilized inductive coupling communication techniques but alignment concerns and the need for higher information rate operation led to studies at UHF frequencies [10], [11] and now there are many commercial solutions available [12]. This interest in RF-based implant communication led to the establishment of the medical implant communication services (MICS) band at 402–405 MHz [5], [13]. More recently, researchers have also been considering the use of the industrial, scientific and medical (ISM) band at 2360–2483.5 MHz due to the ease of antenna design, particularly since WIMD applications are demanding much smaller device dimensions [14]. However, operating at this higher frequency also presents its challenges due to higher wave propagation losses in biological tissues.

There is a significant body of work on UHF antenna design for WIMD applications spanning more than two decades based on PIFA, dipole, loop, monopole, helical and spiral designs [14]–[19], with various techniques to tackle miniaturization whilst maintaining communication link performance [20]. However, most studies tend to present an design optimized for the clinical application being targeted and there are only a few studies covering the *design principles* associated with implant antenna design. Furthermore, the relatively poor radiation performance of implant antenna solutions remains a significant issue [21]. This issue is not helped by the poor link margins in most WIMD systems where regulatory restrictions and battery-based or energy-harvesting powering solutions prevail. The recent drive for more aggressive device miniaturization only exacerbates the situation. Therefore, there is a need for more quantitative consideration of UHF implant antenna performance.

Implant antennas are typically embedded in biological tissues with relatively thin insulating layers. With such lossy dielectric material in its reactive near zone, an antenna's current distribution is modified directly affecting its performance characteristics including return loss [19] and link efficiency since both the radiating (propagating) and reactive field components contribute to power losses [22]. However, propagating component losses are a direct function of the application itself since they depend on antenna position and orientation, and arrangement of the tissue structures themselves. For effective antenna design there needs to be a performance assessment of the *intrinsic* efficiency of the antenna and the design process should seek to minimize both near-field and structural losses since the propagating losses are largely constrained by the application. Traditional antenna radiation efficiency, which is the ratio of total radiated power at any point to input power, is only applicable if the antenna is radiating in a lossless region. For antennas in lossy media an alternative approach is to consider the radiated power at a specific enclosed surface and

Scanlon is with Tyndall National Institute, University College Cork (Ireland) and the remaining authors are with the Centre for Wireless Innovation, ECIT, Queen's University of Belfast (UK).

use this to evaluate performance [23]. Taking this approach we introduce the new concept of *intrinsic radiation efficiency* and based on theoretical analysis we provide practical guidance on how to evaluate this parameter for electrically small UHF implant antennas. The paper is structured as follows. Section II discusses radiation efficiency and Section III the radian length of electrically small antennas in lossy media. Section IV introduces the definition of intrinsic radiation efficiency. Sections IV and V describe illustrative numerical simulation setup and results, respectively. The paper concludes in Section VI with a discussion on how this new approach may be used within numerical simulation and measurement studies.

II. Implant Antenna Efficiency

As the power accepted by an antenna is dissipated either through radiation (P_{rad}) or losses (P_{loss}) in the antenna structure and surrounding environment, radiation efficiency RE is conventionally defined as follows [21]:

$$RE = \frac{P_{rad}}{P_{rad} + P_{loss}} \tag{1}$$

In the context of WIMDs, total losses include 1) ohmic and dielectric losses in the antenna and its packaging, which may include the device circuitry and any bio-compatible insulation; 2) losses in surrounding biological tissues due to reactive near field components that may exist outside of the WIMD packaging [24]; and 3) propagating field component losses [25] which will include both path loss and tissue boundary effects due to wave impedance transition reflections. The first source of loss can only be properly assessed after the WIMD design has been finalized but nonetheless, modern materials and high accuracy simulation tools allow designers to evaluate designs and significantly reduce structural and packaging losses. However, as device dimensions move towards the millimeter and sub-millimeter scale, UHF antennas are not only closer to lossy tissues, but they are more electrically small with more dominant reactive field components. Depending on the local tissue conductivity characteristics and operating frequency, this second category of losses can be quite significant. To some extent, the wave propagation losses are determined fully by the application and independent of the antenna type or its structure. Each propagating wave component is individually affected by the material properties along its path. Several studies have been conducted in the past with the objective of modeling this path loss across single layered and multi-layered tissues [26], [27]. One way of addressing this third source of loss would be to direct wave propagation through less lossy tissues or towards the more direct path to the body surface [28].

Since implantable antennas are required to have a bio-compatible coating [24], this insulating layer also be used to maintain an antenna's performance and prevent close coupling with high conductivity of body tissues [29]. Additionally, insulated antennas have the advantage of being less sensitive to the dielectric properties of the surrounding medium [30]. In [24], it was also emphasized that an insulating bio-compatible layer also has a significant advantage in radiation performance as it helps smooth the wave impedance transition between the source domain and proximate body tissues which typically have quite different dielectric properties [31].

Since the effectiveness of insulating coatings is significantly reduced as they become thinner the drive for much smaller overall package design means that there is also an opportunity to improve WIMD antenna performance by considering antenna design techniques for minimizing near-field tissue losses [32]. Indeed, this issue has also been of interest in the context of reducing the thermal energy absorbed by the surrounding tissues and improving the Specific Absorption Rate [33]. Others have also considered the near field losses in underground antennas [34], and more generally the performance of antennas inside any lossy medium [23]. Therefore, irrespective of the motivation, the importance of near-field tissue losses in implanted antenna applications is well established.

III. Radian Length for Tissue Implanted Source

Wheeler defined the radian sphere as the boundary separating the near field and far field, with a radius, r, of one radian length (r_l) where the three terms of the field for a Hertzian dipole are equal in magnitude [35]. An electrically small antenna (ESA) is then one which is smaller in size than its radian sphere [23]. Such an antenna has a small power factor of radiation which implies that its radiation resistance is much smaller than the principal component of its self-reactance. Consider the field equations of an infinitesimal electric dipole source in lossy material [36]:

$$E_\theta = \frac{IdL}{4\pi(\sigma + j\omega\varepsilon)} \frac{\sin\theta}{r^3} \left(1 + \gamma r + \gamma^2 r^2\right) e^{-\gamma r} \tag{2}$$

$$E_r = \frac{IdL}{2\pi(\sigma + j\omega\varepsilon)} \frac{\cos\theta}{r^3} \left(1 + \gamma r\right) e^{-\gamma r}$$

$$H_\phi = \frac{IdL}{4\pi} \frac{\sin\theta}{r^2} \left(1 + \gamma r\right) e^{-\gamma r}$$

$$\gamma = \left(-\varepsilon\mu\omega^2 + j\omega\mu\sigma\right)^{1/2} \tag{3}$$

The current element is an insulated wire of length dL carrying a uniform current I, which varies harmonically with time with an angular frequency of ω. The complex propagation constant γ is defined in (3) with its real part positive, while the medium is defined by absolute dielectric permittivity ε, absolute magnetic permeability μ and electrical conductivity σ. The distance between the source and the observation point is defined as r. The non-zero spherical components of the electric field intensity and the magnetic field intensity are E_θ, E_r, and H_ϕ, respectively. Similar derivations apply to magnetic antennas using the fields generated by an infinitesimal magnetic dipole immersed in a homogeneous conducting medium such as seawater in spherical coordinates as described in [25].

To determine the radian length, the absolute value of the reactive field components in (2) associated with the r^3 term are equated with the r^2 term.

$$|\gamma| = \left|\frac{1}{r_l}\right|$$

$$r_l = \frac{1}{\left\{(-\varepsilon\mu\omega^2)^2 + (\omega\mu\sigma)^2\right\}^{1/4}} \tag{4}$$

With some manipulation and using the substitutions from [37], (4) can be restated in terms of the wavelength in the medium, λ_g as:

$$\begin{aligned} r_l &= \frac{1}{(((-\frac{2\pi}{\lambda_g})^2)^2 + (((\frac{2\pi}{\lambda_g})^2)\frac{\mu\sigma^2}{\varepsilon}))^{1/4}} \\ &= \frac{1}{((\frac{2\pi}{\lambda_g})^2((\frac{2\pi}{\lambda_g})^2 + \frac{\mu\sigma^2}{\varepsilon}))^{1/4}} \\ &= \frac{1}{\sqrt{\frac{2\pi}{\lambda_g}}(\frac{4\pi^2}{\lambda_g{}^2} + \frac{\mu\sigma^2}{\varepsilon})^{1/4}} \\ &= \frac{\sqrt{\lambda_g}}{\sqrt{2\pi}(\frac{4\pi^2}{\lambda_g{}^2} + \frac{\mu\sigma^2}{\varepsilon})^{1/4}} \\ &= \frac{\sqrt{\frac{\lambda_g}{2\pi}}}{((\frac{2\pi}{\lambda_g})^2 + \frac{\mu\sigma^2}{\varepsilon})^{1/4}} \end{aligned} \tag{5}$$

Further simplification is obtained by splitting the propagation constant into real and imaginary terms and using the binomial expansion to find β and α:

$$\gamma = \alpha + j\beta \tag{6}$$

$$\beta = \omega\sqrt{\mu\varepsilon}\left(\frac{1}{2} + \frac{1}{2}\sqrt{1 + \frac{\sigma^2}{\omega^2\varepsilon^2}}\right)^{\frac{1}{2}} \tag{7}$$

$$\alpha = \frac{\omega\mu\varepsilon}{2\beta} \tag{8}$$

Since human body tissues are a good insulator at UHF ($\sigma << \omega\varepsilon$) we can write:

$$\beta \approx \omega\sqrt{\mu\varepsilon}\left(1 + \frac{\sigma^2}{8\omega^2\varepsilon^2}\right)$$

And since:

$$\tan\delta = \frac{\sigma}{\omega\varepsilon} < 0.5$$

The terms can then be simplified to:

$$\beta \approx \omega\sqrt{\mu\varepsilon}$$

$$\alpha \approx \frac{\sigma}{2}\sqrt{\frac{\mu}{\varepsilon}} = \frac{\beta}{2}\frac{\sigma}{\omega\varepsilon}$$

Therefore, (5) can be approximated as:

$$|\gamma| = \sqrt{\beta^2 + \alpha^2}$$

$$|\gamma| = \beta\sqrt{1 + \frac{\sigma^2}{4\omega^2\varepsilon^2}}$$

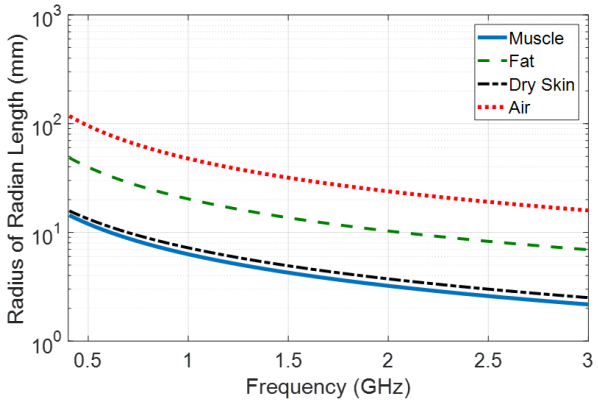


Fig. 1: Exact radian length (Eqn. 5) for selected human tissues.

TABLE I: RMSE for exact (Eqn. 5) and lossless approximation (Eqn. 10) of radian length

Frequency Range (GHz)	Muscle	Fat	Skin
Entire range: 0.4–3.0	5.1%	1.6%	7.2%
Mid range: 0.4–1.4	5.2%	1.6%	7.3%
Low range: 0.4–0.5	7.2%	2.2%	8.8%

$$|\gamma| = \frac{2\pi}{\lambda_g}\sqrt{1 + \frac{\sigma^2}{4\omega^2\varepsilon^2}}$$

$$r_l = \frac{\lambda_g}{2\pi}\left(1 + \frac{\sigma^2}{4\omega^2\varepsilon^2}\right)^{\frac{-1}{2}} \approx \frac{\lambda_g}{2\pi}\left(1 + \frac{\sigma^2}{8\omega^2\varepsilon^2}\right) \tag{9}$$

Equation (9) highlights the relationship between wavelength in the medium and the radian length. For lossless media ($\sigma = 0$), the radian length r_l simplifies to:

$$r_l = \lambda_g/2\pi \tag{10}$$

Equation (5) was used to evaluate the radian length for muscle, fat and dry skin across typical implant antenna frequencies (0.4–1.5 GHz) using dielectric properties based on the parametric model in [38], (Fig. 1). High permittivity tissues have significantly shorter radian lengths. The effect of conductivity on the radian length is not as significant, as demonstrated in Fig. 2. Here the radian length for normal muscle is compared with double loss (2σ) and zero loss ($\sigma = 0$) cases. These non-physical comparisons show that, over typical UHF frequencies and for the widest range of tissue conductivity expected, conductivity is only a significant factor at lower frequencies. Additionally, the use of the lossless simplification (Eqn. 10) is a reasonable approximation as it results in less than 10% root mean square error (RMSE) even for high permittivity, high conductivity tissues (Table I).

IV. Intrinsic Radiation Efficiency of Implanted Antennas

A new figure of merit for UHF implant antennas is proposed. Intrinsic Radiation Efficiency (IRE) is a measure of an implant antenna's ability to efficiently convert accepted power

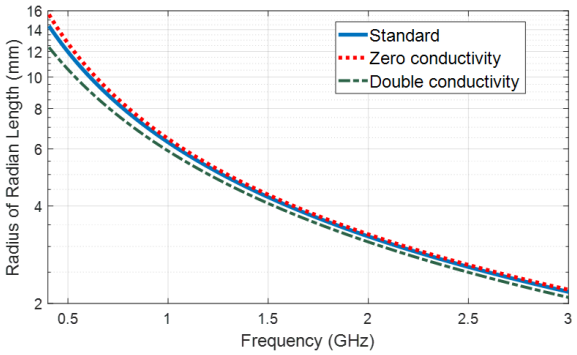


Fig. 2: Exact radian length in muscle equivalent tissues with varying conductivity value.

to propagating wave power within the surrounding human body tissues or an equivalent phantom. If the power accepted by the antenna is P_{acc} and the total power dissipated in the antenna structure and surrounding tissues due to the reactive near field is given by P_{nf}, then:

$$IRE = \frac{P_{acc} - P_{nf}}{P_{acc}} \tag{11}$$

For practical antennas in lossless media (11) is equivalent to (1), i.e., $IRE = RE$. However, for implant antennas RE will always be less than IRE since the radiated power component of (1) is conventionally calculated or measured external to the human body or tissue equivalent phantom. However, even for the same antenna, RE can vary with implantation depth and position since the external radiated power is reduced by both the near-field losses in the antenna and surrounding tissues and also wave propagation losses within the phantom itself. Consider an antenna under test at the center of a homogeneous spherical tissue equivalent phantom much larger than the antenna. If the antenna is moved much closer to the phantom edge, the total radiated power will typically increase leading to an increase in RE, whereas if it is calculated correctly, IRE should not increase. Of course, for implant antennas, determining the radiated power external to the body or tissue equivalent phantom surrounding the implant is consistent with the requirements of most WIMD applications where the overall link budget needs to be evaluated. In contrast, however, the purpose of the new figure of merit is to facilitate the evaluation of the quality of a particular antenna design since reactive near field losses should be minimized. The IRE metric also provides a method of comparing antenna designs between different laboratories and across different applications.

A. Numerical Investigation

A series of simulations were performed in CST Microwave Studio® to investigate techniques for evaluating IRE. An electrically-small dipole antenna encapsulated with an insulating layer was modeled at the center of a finite spherical tissue equivalent phantom (of radius 100 mm and 200 mm), as shown in Fig. 3. Homogeneous muscle and fat tissue phantoms were used as their dielectric properties are quite distinct from each

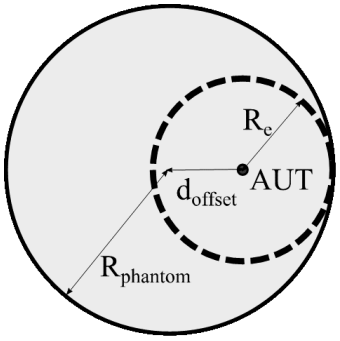


Fig. 3: Schematic of simulation model: the radius of the spherical phantom is $R_{phantom}$, the AUT may be offset within the phantom by distance d_{offset}. Power flow within a sphere of radius R_e, which is always less than $R_{e,max} = R_{phantom} - d_{offset}$, is used to determine IRE.

TABLE II: Simulated Tissue Properties [38]

Phantom	Band	Conductivity (Sm^{-1})	Relative Permittivity
Fat	MICS	0.04	5.58
	ISM	0.10	5.28
Muscle	MICS	0.80	57.1
	ISM	1.71	52.8

other. In total, there are 8 different scenarios in the numerical study, as a set of 2 different phantoms, 2 frequency bands and 2 antenna sizes were used.

For simplicity, the antenna was constructed from a perfect electric conductor (PEC) and the insulation material was a vacuum. While the canonical antenna model and the material characteristics are not particularly realistic, this approach allowed the analysis to focus on the near field tissue losses since there are no antenna structure and packaging losses.

Two distinct frequency bands and two homogeneous phantom tissue types were considered and, to illustrate the use of IRE in antenna design, two different antenna lengths were tested in each scenario. The 402–405 MHz MICS band was chosen as it is specified in IEEE standard 802.15.6-2012 for in-body area networks [39]–[42]. The second frequency band chosen was the 2360–2483.5 MHz band, commonly referred to as the 2.4 GHz ISM band [40], [42]. As discussed in [22], these two bands are the most commonly used for implant communications. The spherical phantoms had a radius of either 100 mm or 200 mm and were homogeneous with either muscle or fat tissue mimicking dielectric properties (Table II). The calculated radian lengths for these dielectric properties and frequencies are given in Table III.

The insulated electrically small dipole antenna model is

TABLE III: Exact (5) and approximated (10) radian length

Phantom	Band	Exact r_l (mm)	Approximated r_l (mm)
Fat	MICS	48.6	49.9
	ISM	8.6	8.6
Muscle	MICS	14.4	15.6
	ISM	2.7	2.7

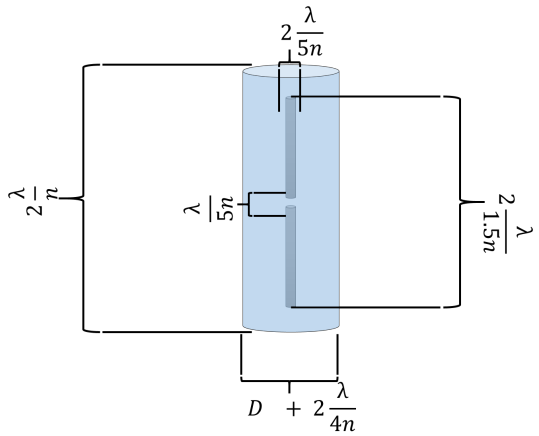


Fig. 4: Schematic of insulated dipole antenna.

similar to the one presented in [43] with a PEC wire radius and a total length dependent on the wavelength in free space. The antenna model was placed at the geometric center of the spherical phantom and the insulation layer was modeled as a vacuum cylinder rather than the sphere used in [43]. The antenna length and the radius of the insulation were varied using a design factor, n, as shown in the schematic in Fig. 4. In the schematic, λ is the free space wavelength in each band (MICS or ISM) and D is the diameter of antenna wire, itself a function of n which was set to either 50 or 82.

V. Results and Discussion

The overall electromagnetic power flow for the simulation model can be computed using the Poynting vector equation [23] and directly obtained in CST Microwave Studio® using the power flow monitor over an enclosed surface. The power flow monitor records the Poynting vector and reports the maximum value of the power flow at every spatial point, encountered within one period of time. Here the surface was chosen to be an enclosed sphere centred on the antenna feed point with a radius R_e, which is always less than $R_{e,max}$ so that the power flow surface is always within the spherical phantom, irrespective of the position of the antenna, which may be offset from the phantom centre (Fig. 3).

Table IV shows the power flow at a radius equal to the exact radian length (Table III) for each combination of antenna size, operating band and tissue type. The values shown are normalized against the accepted input power of each antenna so the values are in dB relative to the accepted power which is the power delivered to the antenna structure taking account of mismatch losses. In all cases, the larger antenna ($n = 50$) always performs better than the smaller one, consistent with less reactive near field losses up to the radian length radius.

Direct comparison between power flow in both tissue types is difficult for the results in Table IV as the radian lengths are so different. Furthermore, since conductivity of fat is so low, the reactive near field region extends much further into the fat phantom. As the antennas under test are very electrically small, they are highly reactive and this combination means that near field losses in fat are potentially more significant than might be expected.

A. Estimating Intrinsic Radiation Efficiency

To better investigate the losses involved, we can plot a graph of power flow versus radial distance, normalized by accepted power (Fig. 5). These results do not distinguish between reactive near field and propagating wave components as both elements are present to some extent in all regions surrounding the antenna. One approach to determining IRE in homogeneous media is to compensate for the expected propagating wave components so that power flow normalized to accepted power becomes a direct measure of structural and near-field tissue losses. Plane wave propagation in homogeneous lossy media is well understood and commonly articulated as depth of penetration, defined as the distance in the medium in which the wave amplitude of a traveling electromagnetic wave is reduced to $1/e$ of its initial value [44]. The depth of penetration (δ) is given by [45]:

$$\delta = \left(\frac{k^2}{2} \left(\sqrt{{\varepsilon_\mathrm{r}}^2 + (\frac{\sigma}{\omega\varepsilon_0})^2} - \varepsilon_\mathrm{r} \right) \right)^{-\frac{1}{2}} \tag{12}$$

This equation can be used to estimate the propagation loss, PL at a distance d (m) for the simulated materials and frequencies using:

$$PL(dB) = 8.686d \left(\frac{1(Np)}{\delta(m)} \right) \tag{13}$$

The attenuation per mm was calculated for each case using (13) and presented in Table V. As there are no losses in the antenna structure or insulation in the simulation model, the normalized power flow results in Fig. 5 can be modified to compensate for the theoretical propagation loss expected at radial distances up to R_e from the source antenna, directly estimating IRE. Since IRE should be constant, any deviation indicates that non-propagating loss mechanisms are still present at that particular radial distance.

Fig. 6 presents the same data given in Fig. 5 but with an assumed theoretical propagation loss (PL, Table V) removed at each data point (10 mm intervals) according to the radial distance involved. For the fat phantom (left graph), the ISM

TABLE IV: Normalised power flow at a radius of r_l

Phantom	Band	Antenna size	Power flow at r_l (dB)
Fat	MICS	$n = 82$	-23.1
		$n = 50$	-16.4
	ISM	$n = 82$	-18.2
		$n = 50$	-12.0
Muscle	MICS	$n = 82$	-8.4
		$n = 50$	-3.3
	ISM	$n = 82$	-7.9
		$n = 50$	-3.2

TABLE V: Theoretical propagation loss, PL (13)

Phantom	Band	PL (dB/mm)
Fat	MICS	0.03
	ISM	0.08
Muscle	MICS	0.16
	ISM	0.38

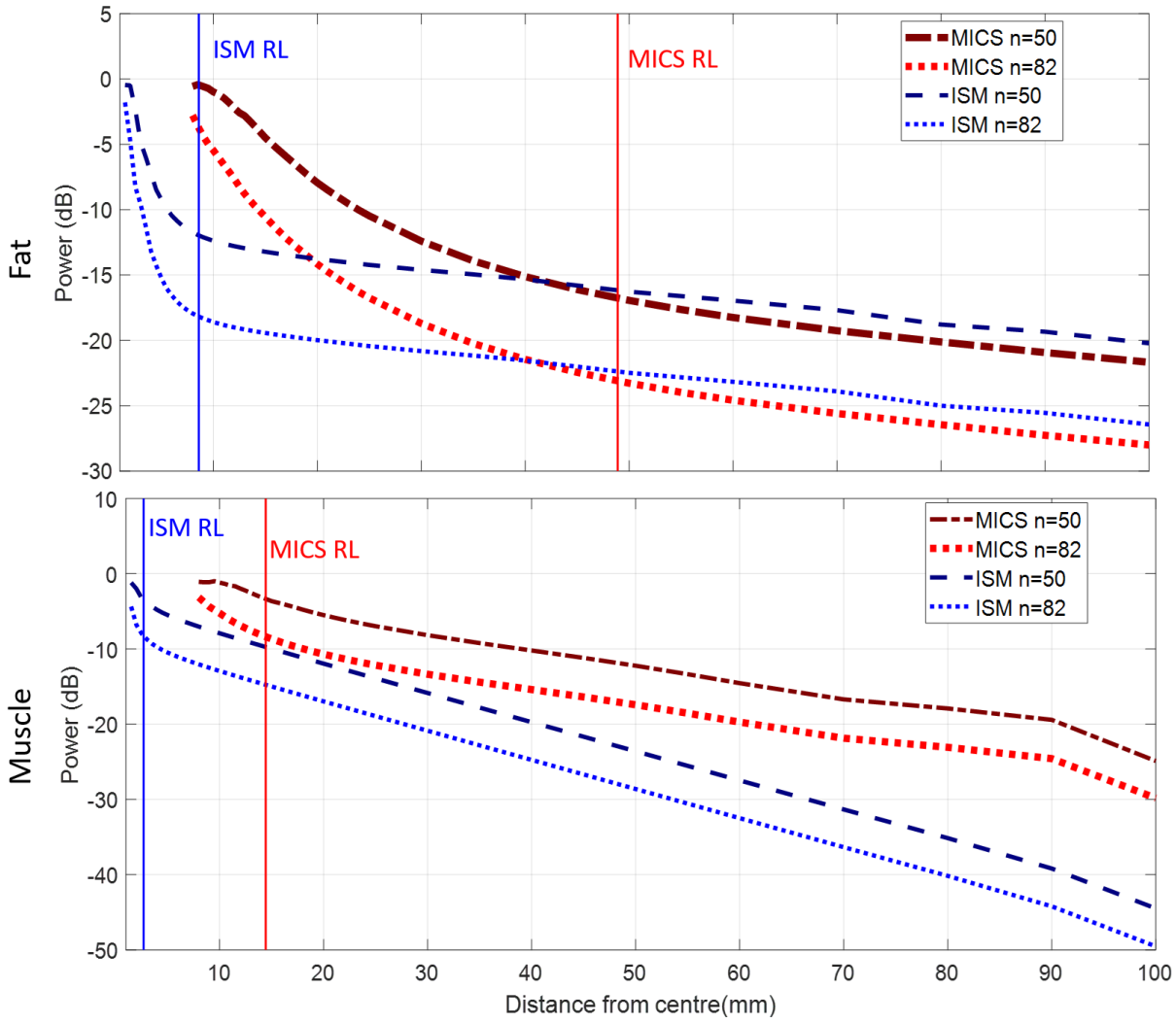


Fig. 5: Normalized power flow versus radial distance for fat (top) and muscle (bottom). The vertical lines represent the exact radian length for each case.

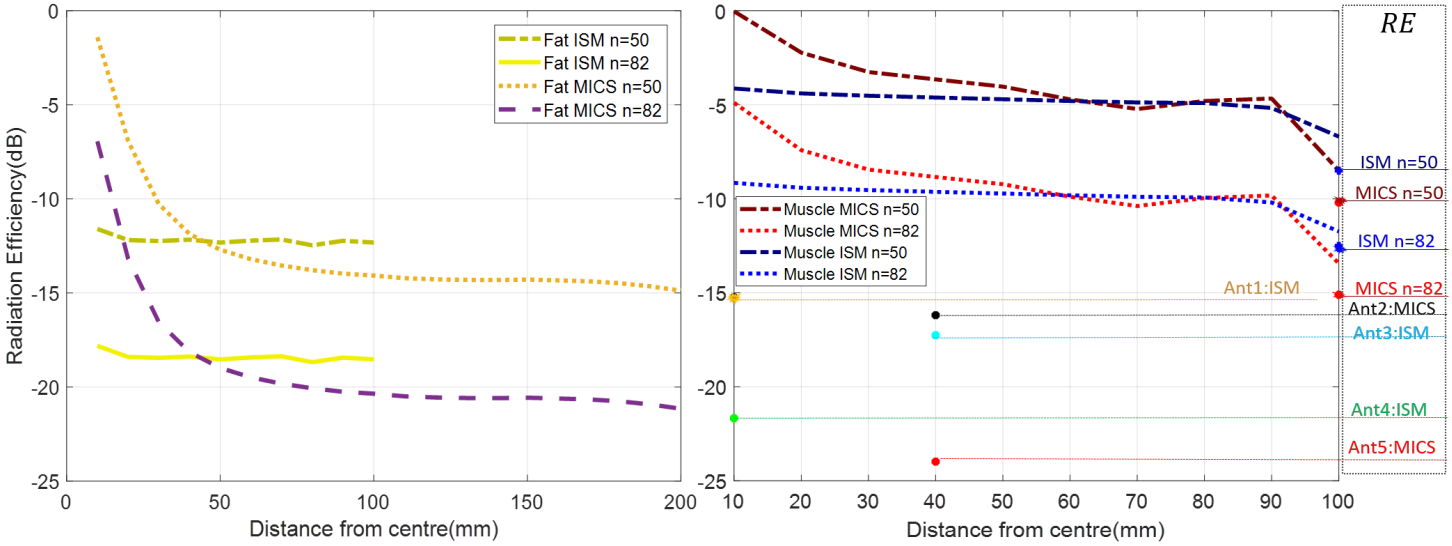


Fig. 6: IRE estimates versus radial distance for both fat (left) and muscle (right) phantoms. The muscle chart includes IRE of antennas in the literature; Ant1: [46], Ant2: [47], Ant3: [47], Ant4: [46] and Ant5: [48].

band results show a relatively constant estimated IRE at all distances significantly beyond r_l (8.6 mm) with around 6 dB advantage for the larger antenna (Table VI). The low permittivity of the fat equivalent medium also means that there are no significant boundary effects at the phantom edge (100 mm). However, for the MICS band, the radian length is over five times larger (48.6 mm) and the estimate of IRE does not settle within the original phantom radius ($R_{\text{phantom}} \approx 2r_l$). Therefore, a phantom with a larger radius ($R_{\text{phantom}} = 200$ mm) was used for this case. Again, the larger antenna performs better, with a 6 dB advantage developing outside the reactive near-field zone. The muscle phantom results (right graph) are also interesting. Again, for the ISM band, there is a relatively constant IRE but unlike the fat case there are strong boundary effects towards the edge of the phantom. This is consistent with the significant change in wave impedance encountered. In the lower frequency MICS case it is also apparent that the IRE estimate only settles beyond several radian lengths ($r_l = 14.4$ mm) and the boundary effect is even more pronounced. This is consistent with the higher reflection coefficient associated with the increased permittivity at 400 MHz.

The IRE values are consistently higher in the muscle phantom than in the fat phantom (≈ 15 dB higher at MICS and ≈ 8 dB at ISM band). This reflects the significantly shorter radian length in muscle than in fat due to the much higher permittivity. Even though the conductivity of muscle is higher than fat, this reduction in the volume of the reactive near-field zone leads to overall reduced losses in the non-propagating wave components. These results also show that operation at the higher frequency ISM band can be advantageous. In the fat case, IRE increases and the relatively low propagation constant in this medium means that performance actually increases as shown in the power flow results (Fig. 5). For the muscle case, the IRE is approximately the same at both MICS and ISM. However, propagation losses quickly grow with frequency. This means that there is a direct trade-off in terms of operating frequency, implant size and implant depth since a higher frequency means that for a fixed package size, the antenna is electrically larger and, depending on the distance from implant to surface, the higher IRE might more than account for the additional path loss incurred. Furthermore, all aspects of antenna engineering are less challenging as the electrical size of the problem increases.

Moreover, all of these results indicate that estimation of IRE by considering power flow and compensating for propagation losses is extremely useful but that care is needed to ensure that the estimate is made sufficiently far from the antenna under test to ensure that near field losses are sufficiently diminished to become negligible. Based on the results presented here, it is recommended that this minimum distance, R_{min}, is set as πr_l:

$$R_{\text{min}} = \pi r_l \approx \frac{\lambda_{\text{g}}}{2}. \tag{14}$$

Furthermore, IRE needs to be evaluated in a phantom of sufficient size, with a minimum radius from the antenna structure larger than the evaluation radius of (14) to also ensure that boundary wave impedance effects are minimized. This minimum distance restriction applies regardless of the shape of the phantom and the relative position of the antenna under evaluation. To illustrate, the IRE of the ISM antenna in the muscle homogeneous phantom was determined for three different positions along the radial ($d_{\text{offset}} = 0, 10, 50$ mm) direction. The results are shown in Fig. 7 and IRE for the recommended radial distance (R_{min}) is presented in Table VII. The IRE results are effectively unaffected by any offset (as πr_l is within the phantom for all three offsets). This highlights the robustness of this figure of merit.

It is also possible to estimate IRE using conventional RE results obtained external to a homogeneous phantom by measurement or simulation. However, these results will always be lower than IRE estimates obtained via the recommended power flow compensated method due to the reflection loss incurred at the external phantom boundary. In Fig. 6 the right hand graph has symbols placed on the $x = 100$ mm axis. These are IRE values estimated using CST reported conventional radiation efficiency results and taking account of the expected propagation loss in 100 mm of phantom. This approach also allows comparison with results from other laboratories where different phantom dimensions were used. The right hand graph of Fig. 6 also shows estimated IRE data points at $x = 40$ mm and $x = 10$ mm that were obtained using the conventional RE results found in [46]–[48]. These studies considered antennas in both ISM and MICS frequency bands in homogeneous muscle tissue phantoms. Although different phantom shapes were used and the studies considered distinct applications, the use of estimated IRE as a performance metric allows for some limited comparisons.

VI. Conclusion

Consideration of the sources of loss for tissue-implanted UHF antennas has identified the need for a new figure of merit to facilitate quantitative analysis of competing designs.

TABLE VI: Estimated Intrinsic Radiation Efficiency

Phantom	Band	Antenna size	IRE (dB)
Fat	MICS	$n = 82$	≤ -25
		$n = 50$	≤ -19
	ISM	$n = 82$	-18
		$n = 50$	-12
Muscle	MICS	$n = 82$	-10
		$n = 50$	-5
	ISM	$n = 82$	-10
		$n = 50$	-5

TABLE VII: IRE at different radial offset distances (ISM band, muscle phantom.

Antenna size	Offset (mm)	IRE at πr_l (dB)
$n = 50$	0	-4.1
	10	-4.1
	50	-4.1
$n = 82$	0	-9.1
	10	-9.1
	50	-9.1

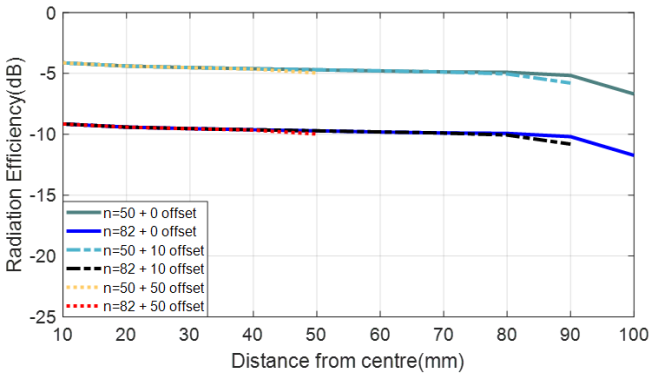


Fig. 7: IRE in muscle phantom with varying offset from the centre of the phantom.

The losses associated with the dominant propagating paths are typically application specific, and at early stages of the design process they are particular to the phantom chosen for empirical or numerical evaluation. To overcome these limitations, the concept of *intrinsic radiation efficiency* is proposed for UHF implant antenna analysis. This new metric takes account of the structural, packaging and near-field dielectric tissue losses associated with an implanted antenna.

To illustrate this new approach, a methodology for estimating intrinsic radiation efficiency using numerical simulation of power flow was presented. The results considered canonical electrically small dipole antennas in homogeneous tissue equivalent phantoms at two common operating frequencies for medical implant communications. As well as demonstrating the utility of the new approach, the results illustrate the challenges of using the MICS band, where the lower frequency and typically higher permittivity values for tissues leads to an extended near field region (longer radian length) that is difficult to constrain within the medical device packaging and insulation in modern miniaturized applications. At higher frequencies, the shorter radian length leads to potentially much lower near-field tissue losses. However, this must be balanced against the significantly higher propagation losses that will be encountered. Ultimately, the antenna design will be a trade off determined largely by the propagation path length involved and the application constrained packaged device size.

While the work presented only considered homogeneous tissue structures, the approach remains valid for more complex scenarios as the fundamental definition of intrinsic radiation efficiency remains unchanged. However, assessment of the total extent of near field losses becomes much more difficult. Nonetheless, numerical code developers can use the concepts presented in this paper to fully automate such processes. In a similar way to the assessment of specific absorption rate, an automated process can take account of any possible tissue structure.

In terms of its use in empirical measurements, intrinsic radiation efficiency could be readily determined in homogeneous phantoms using discrete electric field measurements and a similar methodology of propagating path compensation as presented here for numerical modeling. However, the complexity of these measurements grows rapidly as radiating structures become more irregular and if an inhomogeneous phantom is employed.

This work will lead to improved implant antenna design as engineers will seek to further reduce losses within their control and, for the first time, it enables different laboratories and teams to quantitatively compare their achievements in optimizing implant antennas. Importantly, the latter can be achieved without resort to a single standardized test phantom, thus promoting low cost access to research.

REFERENCES

[1] C. Huang, T. Kawajiri, and H. Ishikuro, "A 13.56-MHz Wireless Power Transfer System With Enhanced Load-Transient Response and Efficiency by Fully Integrated Wireless Constant-Idle-Time Control for Biomedical Implants," *IEEE Journal of Solid-State Circuits*, vol. 53, no. 2, pp. 538–551, Feb 2018.

[2] M. Wazid, A. K. Das, N. Kumar, M. Conti, and A. V. Vasilakos, "A Novel Authentication and Key Agreement Scheme for Implantable Medical Devices Deployment," *IEEE Jnl. of Biomedical & Health Informatics*, vol. 22, no. 4, pp. 1299–1309, Jul 2018.

[3] M. Bosiljevac, Z. Sipus, and A. K. Skrivervik, "Propagation in Finite Lossy Media: An Application to WBAN," *IEEE Antennas & Wireless Propagation Ltrs.*, vol. 14, pp. 1546–1549, 2015.

[4] R. S. Alrawashdeh, Yi Huang, M. Kod, and A. Abu Bakar Sajak, "A Broadband Flexible Implantable Loop Antenna With Complementary Split Ring Resonators," *IEEE Antennas & Wireless Propagation Ltrs.*, vol. 14, pp. 1506–1509, 2015.

[5] C. W. L. Lee, A. Kiourti, and J. L. Volakis, "Miniaturized Fully Passive Brain Implant for Wireless Neuropotential Acquisition," *IEEE Antennas & Wireless Propagation Ltrs.*, vol. 16, pp. 645–648, 2017.

[6] A. Valanarasi and R. Dhanasekaran, "A review on design considerations of implantable antennas," in *Intl. Conf. Advanced Communication Control & Computing Tech. (ICACCCT)*, May 2016, pp. 207–211.

[7] C. Garcia-Pardo, A. Fornes-Leal, N. Cardona, R. Chavez-Santiago, J. Bergsland, I. Balasingham, S. Brovoll, O. Aardal, S.-E. Hamran, and R. Palomar, "Experimental Ultra Wideband Path Loss Models for Implant Communications," in *27th Annual Intl. Symp. Personal, Indoor & Mobile Radio Communications (PIMRC)*, Sep 2016, pp. 1–6.

[8] P. Leelatien, K. Ito, K. Saito, M. Sharma, and A. Alomainy, "Channel Characteristics and Wireless Telemetry Performance of Transplanted Organ Monitoring System Using Ultrawideband Communication," *IEEE Jnl. Electromagnetics, RF & Microwaves in Medicine & Biology*, vol. 2, no. 2, pp. 94–101, Jun 2018.

[9] A. Kiourti, C. W. L. Lee, J. Chae, and J. L. Volakis, "A Wireless Fully Passive Neural Recording Device for Unobtrusive Neuropotential Monitoring," *IEEE Trans. Biomedical Engineering*, vol. 63, no. 1, pp. 131–137, Jan 2016.

[10] M. N. Islam and M. R. Yuce, "Review of Medical Implant Communication System (MICS) band and network," *ICT Express*, vol. 2, no. 4, pp. 188–194, Dec 2016.

[11] Basari, D. C. Sirait, F. Y. Zulkifli, and E. T. Rahardjo, "A Helical Folded Dipole Antenna for Medical Implant Communication Applications," in *IEEE MTT-S Intl. Microwave Workshop Series on RF & Wireless Technologies for Biomedical & Healthcare Applications (IMWS-BIO)*, Dec 2013, pp. 1–3.

[12] Microsemi Corporation, "Microsemi's New RF Modules Speed Time to Market for Implantable Medical Device Designers," 2018. [Online]. Available: https://www.prnewswire.com/news-releases/microsemis-new-rf-modules-speed-time-to-market-for-implantable-medical-device-designers-300598841.html

[13] A. Sharma, E. Kampianakis, and M. S. Reynolds, "A Dual-Band HF and UHF Antenna System for Implanted Neural Recording and Stimulation Devices," *IEEE Antennas & Wireless Propagation Ltrs.*, vol. 16, pp. 493–496, 2017.

[14] A. Kiourti and K. S. Nikita, "A Review of In-Body Biotelemetry Devices: Implantables, Ingestibles, and Injectables," *IEEE Trans. Biomedical Engineering*, vol. 64, no. 7, pp. 1422–1430, Jul 2017.

[15] P. Soontornpipit, C. Furse, and Y. Chung, "Design of Implantable Microstrip Antenna for Communication With Medical Implants," *IEEE Trans. Microwave Theory & Tech.*, vol. 52, no. 8, pp. 1944–1951, Aug 2004.

[16] J. Faerber, G. Cummins, S. K. Pavuluri, P. Record, A. R. A. Rodriguez, H. S. Lay, R. McPhillips, B. F. Cox, C. Connor, R. Gregson, R. E. Clutton, S. R. Khan, S. Cochran, and M. P. Y. Desmulliez, "In Vivo Characterization of a Wireless Telemetry Module for a Capsule Endoscopy System Utilizing a Conformal Antenna," *IEEE Trans. Biomedical Circuits & Systems*, vol. 12, no. 1, pp. 95–105, Feb 2018.

[17] M. Manoufali, K. Bialkowski, B. J. Mohammed, P. C. Mills, and A. Abbosh, "Near-Field Inductive-Coupling Link to Power a Three-Dimensional Millimeter-Size Antenna for Brain Implantable Medical Devices," *IEEE Trans. Biomedical Engineering*, vol. 65, no. 1, pp. 4–14, Jan 2018.

[18] K. N. Bocan, M. H. Mickle, and E. Sejdic, "Tissue Variability and Antennas for Power Transfer to Wireless Implantable Medical Devices," *IEEE Jnl. Translational Eng. in Health & Medicine*, vol. 5, pp. 1–11, 2017.

[19] H. Bahrami, S. A. Mirbozorgi, L. A. Rusch, and B. Gosselin, "Biological Channel Modeling and Implantable UWB Antenna Design for Neural Recording Systems," *IEEE Trans. Biomedical Engineering*, vol. 62, no. 1, pp. 88–98, Jan 2015.

[20] A. Skrivervik, J.-F. Zurcher, O. Staub, and J. Mosig, "PCS Antenna Design: the Challenge of Miniaturization," *IEEE Antennas & Propagation Magazine*, vol. 43, no. 4, pp. 12–27, 2001.

[21] C. Pfeiffer, "Fundamental Efficiency Limits for Small Metallic Antennas," *IEEE Trans. Antennas & Propagation*, vol. 65, no. 4, pp. 1642–1650, Apr 2017.

[22] A. K. Skrivervik, "Implantable antennas: The Challenge of Efficiency," in *7th European Conference on Antennas and Propagation (EUCAP)*, Gothenburg, Sweden, 2013.

[23] A. Karlsson, "Physical Limitations of Antennas in a Lossy Medium," *IEEE Trans. Antennas & Propagation*, vol. 52, no. 8, pp. 2027–2033, Aug 2004.

[24] F. Merli, B. Fuchs, J. R. Mosig, and A. K. Skrivervik, "The Effect of Insulating Layers on the Performance of Implanted Antennas," *IEEE Trans. Antennas & Propagation*, vol. 59, no. 1, pp. 21–31, Jan 2011.

[25] C. Uribe and W. Grote, "Radio Communication Model for Underwater WSN," in *3rd Intl. Conf. on New Technologies, Mobility & Security*, Dec 2009, pp. 1–5.

[26] D. Kurup, W. Joseph, G. Vermeeren, and L. Martens, "In-body Path Loss Model for Homogeneous Human Tissues," *IEEE Trans. Electromagnetic Compatibility*, vol. 54, no. 3, pp. 556–564, Jun 2012.

[27] D. Kurup, G. Vermeeren, E. Tanghe, W. Joseph, and L. Martens, "In-to-Out Body Antenna-Independent Path Loss Model for Multilayered Tissues and Heterogeneous Medium." *Sensors*, vol. 15, no. 1, pp. 408–21, Dec 2014.

[28] Y. El-Saboni, G. A. Conway, and W. G. Scanlon, "The Importance of Antenna Near-Field Losses in Intra-Body UHF Communication Applications," in *IEEE Intl. Symp. Antennas & Propagation & USNC/URSI National Radio Science Meeting*, San Diego, 2017, pp. 399–400.

[29] J. Gemio, J. Parron, and J. Soler, "Human Body effects on Implantable Antennas for ISM Bands Applications: Models Comparison and Propagation Losses Study," *Progress In Electromagnetics Research*, vol. 110, pp. 437–452, 2010.

[30] M. Hanson, H. Powell, A. Barth, K. Ringgenberg, B. Calhoun, J. Aylor, and J. Lach, "Body Area Sensor Networks: Challenges and Opportunities," *Computer*, vol. 42, no. 1, pp. 58–65, Jan 2009.

[31] G. Smith, "Directive properties of antennas for transmission into a material half-space," *IEEE Transactions on Antennas & Propagation*, vol. 32, no. 3, pp. 232–246, Mar 1984.

[32] M. Manteghi and A. A. Y. Ibraheem, "On the Study of the Near-Fields of Electric and Magnetic Small Antennas in Lossy Media," *IEEE Trans. Antennas & Propagation*, vol. 62, no. 12, pp. 6491–6495, Dec 2014.

[33] N. Vidal and J. M. López-Villegas, "Changes in Electromagnetic Field Absorption in the Presence of Subcutaneous Implanted Devices: Minimizing Increases in Absorption," *IEEE Trans. Electromagnetic Compatibility*, vol. 52, no. 3, pp. 545–555, Aug 2010.

[34] D. Large, L. Ball, and A. Farstad, "Radio Transmission to and from Underground Coal Mines–Theory and Measurement," *IEEE Trans. Communications*, vol. 21, no. 3, pp. 194–202, Mar 1973.

[35] H. Wheeler, "The Radiansphere around a Small Antenna," *Proceedings of the IRE*, vol. 47, no. 8, pp. 1325–1331, Aug 1959.

[36] R. Gabillard, P. Degauque, and J. Wait, "Subsurface Electromagnetic Telecommunication - A Review," *IEEE Trans. Communication Technology*, vol. 19, no. 6, pp. 1217–1228, Dec 1971.

[37] R. W. Ziolkowski and E. Heyman, "Wave Propagation in Media Having Negative Permittivity and Permeability," *Physical Review E*, vol. 64, no. 5, p. 056625, Oct 2001.

[38] C. Gabriel, "Compilation of the Dielectric Properties of Body Tissues at RF and Microwave Frequencies." 1996.

[39] R. Chavez-Santiago, K. Sayrafian-Pour, A. Khaleghi, K. Takizawa, J. Wang, I. Balasingham, and H.-B. Li, "Propagation Models for IEEE 802.15.6 Standardization of Implant Communication In Body Area Networks," *IEEE Communications Magazine*, vol. 51, no. 8, pp. 80–87, Aug 2013.

[40] R. Chavez-Santiago, C. Garcia-Pardo, A. Fornes-Leal, A. Valles-Lluch, G. Vermeeren, W. Joseph, I. Balasingham, and N. Cardona, "Experimental Path Loss Models for In-Body Communications Within 2.36-2.5 GHz," *IEEE Jnl. Biomedical & Health Informatics*, vol. 19, no. 3, pp. 1–1, 2015.

[41] K. Sayrafian-Pour, W.-B. Yang, J. Hagedorn, J. Terrill, K. Yekeh Yazdandoost, and K. Hamaguchi, "Channel Models for Medical Implant Communication," *Intl. Jnl. of Wireless Information Networks*, vol. 17, no. 3-4, pp. 105–112, Dec 2010.

[42] L. Schmitt, J. Espina, T. Falck, and D. Wang, "Biosensor Communication Technology and Standards," in *Handbook of Biomedical Telemetry*. Hoboken, NJ, USA: John Wiley & Sons, Inc., Aug 2014, pp. 330–367.

[43] J. Lee and S. Nam, "Effective Area of a Receiving Antenna in a Lossy Medium," *IEEE Trans. Antennas & Propagation*, vol. 57, no. 6, pp. 1843–1845, Jun 2009.

[44] A. Ghasemi, A. Abedi, and F. Ghasemi, "Basic Principles in Radiowave Propagation," in *Propagation Engineering in Wireless Communications*. New York, NY: Springer New York, 2012, ch. 2, pp. 23–55.

[45] K. Siwiak, *Radiowave Propagation and Antennas for Personal Communications*. Artech House, 2007.

[46] M.-R. Tofighi and S.-M. Huang, "Radiation efficiency of planar implantable antennas at ISM band," in *IEEE Topical Conf. Biomedical Wireless Technologies, Networks, & Sensing Systems (BioWireleSS)*, Jan 2014, pp. 43–45.

[47] F. Merli, L. Bolomey, J. F. Zürcher, G. Corradini, E. Meurville, and A. K. Skrivervik, "Design, Realization and Measurements of a Miniature Antenna for Implantable Wireless Communication Systems," *IEEE Trans. Antennas & Propagation*, vol. 59, no. 10, pp. 3544–3555, Oct 2011.

[48] D. Nikolayev, M. Zhadobov, P. Karban, and R. Sauleau, "434 MHz ISM band antenna for in-body biotelemetry capsules," in *11th European Conf. Antennas & Propagation (EUCAP)*, Mar 2017, pp. 1035–1038.



Yomna El-Saboni received her B.Sc. degree in electrical engineering with a minor in biomedical engineering from the American University of Sharjah, UAE in 2013 and her M.Sc. in medical engineering from the University of Leeds, UK in 2014. She is currently working on her Ph.D. degree in Electronic Engineering in the area of medical implant wireless body-centric communications and sensors. Her research interests include miniaturized medical implantable devices and robotics, electrically small implantable antennas, computational electromagnetism for biomedical applications and wireless communication between several implantable devices within the human body.



Dmitry Zelenchuk (M'05–SM'14) received the Ph.D. degree in radiophysics from Rostov State University, Rostov, Russia, in 2004. From 2003 to 2005, he was a Lecturer with the Department of Applied Electrodynamics and Computer Modelling, Rostov State University, Russia. Currently, he is a Lecturer with the Centre for Wireless Innovations, ECIT, Queen's University Belfast, U.K. His research interests include electromagnetic field theory, material characterization, propagation in complex environments, including in- and on-body propagation, millimeter-wave circuits, antennas, and advanced packaging, and various physical phenomena of plasmonic and nanostructures. He has authored and co-authored more than 100 journal and conference papers and a book chapter and been a session chair at scientific conferences.



Gareth A. Conway received a BEng Hons. degree in Electronic Systems from Ulster University, UK in 2004. In 2008, he completed a Ph.D. degree in Electronic Engineering, entitled 'Wearable Antennas for On-Body Wireless Communications' at Queen's University of Belfast, (UK). On completion of his doctorate, he spent three years as a commercial research engineer, specializing in antennas and propagation for mobile communication. In 2011, he rejoined QUB to complete an EPSRC Knowledge Transfer Secondment with Toumaz Healthcare Ltd., undertaking research and development in 'Innovative body-worn antennas for medical devices.' In 2013 he became a Lecturer in Communications Engineering at ECIT, Queens University of Belfast. Dr. Conway has authored or co-authored 45 international conference and journal papers. His research interests include antennas, human tissue equivalent materials, wave propagation and computational electromagnetism for wearable and implantable communications.



William G. Scanlon (M'98–SM'13) is a Professor and Chief Executive Officer at Tyndall National Institute, University College Cork, Ireland. He had previously been Senior Lecturer and Full Professor at Queen's University of Belfast (UK, 2002–2018) and held leadership positions such as Director of the Centre for Wireless Innovation and Head of School of Electronics, Electrical Engineering and Computer Science. He held a part-time Chair in Short Range Radio at the University of Twente, The Netherlands (2009–2014). Scanlon is a pioneer in wearable and implantable medical device communications. He was a Series Editor of the IET Book Series on Telecommunications and Networking, an inaugural Associate Editor of IEEE Journal of Translational Engineering in Health and Medicine and an Associate Editor for IEEE Antennas and Wireless Propagation Letters. He holds an URSI Young Scientist award (1999), the 2010 IEEE H. A. Wheeler Prize Paper Award and he delivered the 2012 NATO Intl. Lecture Series on Next Generation Communications.